Cellulose (2024) 31:5635–5651
https://doi.org/10.1007/s10570-024-05950-5

ORIGINAL RESEARCH

Emulsions, dipsticks and membranes based on oxalic acid-treated nanocellulose for the detection of aqueous and gaseous $HgCl_2$

Gabriela A. Bastida · Roberto J. Aguado · Núria Fiol · Marc Delgado-Aguilar · Miguel Á. Zanuttini · María V. Galván · Quim Tarrés

Received: 27 December 2023 / Accepted: 8 May 2024 / Published online: 25 May 2024

Abstract Although cellulosic materials have been used as stabilizing agents for oil-in-water emulsions since the 1980s, their properties and the underlying mechanism are not universal regardless of the dispersed phase or of the treatments on cellulose. One case of unconventional organic phase is acetic acid-containing chloroform, which is known to be a good solvent system for the preservation of dithizone. In turn, dithizone is a long-known chromogenic reagent for the colorimetric detection of $HgCl_2$. However, its usefulness is limited by its fast degradation in polar solvents. For instance, its dissolution in ethanol and the subsequent impregnation of paper strips allowed to quantify aqueous $HgCl_2$ reliably and quickly (5.4 – 27 mg L^{-1}), but only if they were used along the first 24 h after dip coating. Furthermore, those strips could not be used for sublimated $HgCl_2$. The dithizone/chloroform-in-water emulsions presented in this work overcame these limitations. We opted for oxalic acid-treated cellulose nanofibers (ox-CNFs) as stabilizer, aiming at a proper balance between amphiphilic character and electrostatic repulsion. In this sense, ox-CNFs attained good gel-forming ability with a low content of carboxylate groups. The minimum ox-CNF concentration required was 0.35 wt%, regardless of the proportion of chloroform. This consistency implied yield stress values above 0.7 Pa. Nanocellulose also provided film-forming capabilities, which were exploited to produce visually responsive dipsticks and membranes. While quantification and reproducibility were hampered by the increase in the complexity of the system, dithizone/ox-CNF films were still a valid option for $HgCl_2$ detection, outperforming solution coating in terms of stability, blank signal, and selectivity.

Keywords Colorimetric detection · Dithizone · Heavy metals · Mercury(ii) chloride · Nanocellulose · Oxalic acid

Abbreviations

∀	As long as
$\dot{\gamma}$	Shear rate
θ	Oil/solid/water angle
τ	Shear stress
BEP	Bleached eucalyptus pulp
DTZ	Dithizone
IFT	Interfacial tension

Supplementary Information The online version contains supplementary material available at https://doi.org/10.1007/s10570-024-05950-5.

G. A. Bastida · R. J. Aguado (✉) · N. Fiol · M. Delgado-Aguilar · Q. Tarrés
LEPAMAP-PRODIS Research Group, University of Girona, M Aurèlia Capmany 61, 17003 Girona, Spain
e-mail: roberto.aguado@udg.edu

G. A. Bastida · M. Á. Zanuttini · M. V. Galván
Instituto de Tecnología Celulósica, Facultad de Ingeniería Química (FIQ-CONICET), Universidad Nacional del Litoral, Santiago del Estero 2654, S3000AOJ Santa Fe, Argentina

LOD	Limit of detection
LOQ	Limit of quantification
Ox-CNFs	Oxalic acid-treated cellulose nanofibers
R	Sauter radius of droplets
TEMPO	2,2,6,6-Tetramethylpiperidine-1-oxy radical
EDTA	Ethylenediaminetetraacetic acid

Introduction

$HgCl_2$ is the most widely used mercury(II) salt in the industry. It is employed to catalyze the conversion of acetylene to vinyl chloride monomer, for the amalgamation of metals, and to stabilize analytical standards, among other applications (Li et al. 2018; Tong et al. 2021). Likewise, it results from the oxidation of Hg_2Cl_2 in calomel electrodes (Tigari et al. 2021). $HgCl_2$ is slightly volatile even at ordinary temperatures, to the extent that it is traditionally known as "corrosive sublimate" (Evans and Looker 1921). At a given temperature (T) below 545 K, the vapor pressure (P) of solid $HgCl_2$ is given by the August equation (Phillips et al. 1959):

$$\log_{10} P\,(mmHg) = 10.67 - \frac{4470}{T(K)} \quad (1)$$

Despite its low volatility at room temperature, two facts should be taken into account. First, $HgCl_2$ is nephrotoxic, hepatotoxic, genotoxic, hemotoxic, neurotoxic, very hazardous to the environment, and prone to bioaccumulation (Sangvanich et al. 2014), so it could be stated that there is no safe level of exposure. Second, industries applying $HgCl_2$ as catalyst, such as that of vinyl chloride, employ temperatures in the 80 – 180 °C range (Li et al. 2019a). In China, regulations adopted in 2012 imposed a transition for $HgCl_2$ loadings in catalysts from 10–12 wt% to 4.5–6 wt%, and pollution due to sublimation has been notoriously reduced since then (Li et al. 2019b). Still, it can be argued that industries using $HgCl_2$, be it in aqueous solution or at temperatures that imply significant sublimation, would benefit from user-friendly and cheap detection systems to improve safety conditions for all workers. For instance, cellulose nanocrystals have been functionalized with rhodamine to become visually responsive to mercury(II) in water (Ye et al. 2020).

Another popular reagent for the colorimetric detection of mercury(II) compounds is 1,5-diphenylthiocarbazone, more familiarly known as dithizone (DTZ) (Naghdi et al. 2020; Aguado et al. 2023a). Generally speaking, it cannot be deemed selective, as at least lead(II), cadmium(II), and zinc ions can trigger a similar color change in solution (Ashizawa et al. 1970). In any case, DTZ has already proven its success in paper-based indicators, using chloroform as solvent and attaining successful quantification of mercury(II) nitrate at trace concentrations (Wang et al. 2018). Addressing the nitrate is not surprising from an analytical point of view, given its higher solubility and its higher ionic character. Nonetheless, as aforementioned, the chloride poses a bigger threat due to its persistent industrial use, its certain volatility, and its higher frequency of appearance in surface waters (Jin et al. 2019).

A previous work of ours addressed the stability issues of DTZ in aqueous systems, approaching them by its solvation in chloroform and the emulsification of DTZ/chloroform droplets in water by means of anionic nanocellulose (Aguado et al. 2023a). Such anionic nanocellulose was produced by oxidizing a bleached cellulosic pulp with (2,2,6,6-tetramethylpiperidin-1-yl)oxyl radical (TEMPO), following a widely reported procedure (Saito and Isogai 2004; Fiol et al. 2019), and fibrillating the oxidized cellulose fibers by high-pressure homogenization. Chloroform's toxicity was admitted being a drawback of the system, but it protected DTZ from degradation, besides being one of the few solvents in which the solubility of DTZ is higher than 10 g/L (Irving and Iwantscheff 1980). Even though the first usage of cellulosic derivatives as Pickering stabilizer dates from the 1980s (Oza and Frank 1986), it has acquired renewed interest as of recently (Yu et al. 2022; Zheng et al. 2022). However, the oil phase is generally highly hydrophobic (Li et al. 2020; Souza et al. 2021; Torlopov et al. 2021), in such way that the high interfacial tension promotes the adsorption of cellulose, preferentially by its (200) planes, on dispersed droplets (Aguado et al. 2023b). The choice of acetic acid-containing chloroform as organic phase presents, thus, interesting challenges.

In this new approach, we opt for similar emulsions to produce films or membranes for the detection of both gaseous and aqueous $HgCl_2$, following the current trend of optically responsive nanopapers (Sharifi et al. 2022; Tang et al. 2024). For aqueous $HgCl_2$, these materials were compared to paper dipsticks in which chloroform was replaced

with a greener solvent with more affinity towards the substrate: ethanol. However, the colorimetric detection of gaseous $HgCl_2$ relied on its cumulative adsorption onto a DTZ-containing nanopaper. Hence, DTZ required to be solvated with a water-immiscible solvent for the response to the analyte not to be confused with color changes due to tautomerism or degradation (Umar 2022).

In this context, the strategy resorted to the aforementioned emulsions (Aguado et al. 2023a), but choosing an oxalic acid treatment instead of TEMPO-mediated oxidation (Bastida et al. 2022). The resulting nanocellulose (after fibrillation) was expected to resemble the rheological behavior of those TEMPO-oxidized nanofibers, while containing less carboxylate groups. It has been shown that high degrees of oxidation hinder the attachment of dyes that are preferentially adsorbed onto the hydrophobic parts of cellulose (Isogai et al. 2010). This work shows that, even with a low content of charged functional groups, dilute suspensions of oxalic acid-treated nanofibers display yield stress and can effectively stabilize emulsions of dithizone/chloroform in water.

Experimental

Materials

The source of cellulose for nanocellulose oxalate production was bleached eucalyptus pulp (BEP), provided by Suzano Papel e Celulose S.A. (Aracruz, Brazil). The TAPPI Test Method T203 (TAPPI 2020) revealed an α-cellulose content of 70 ± 2 wt%, with β-/γ-cellulose accounting for 27 ± 2 wt%. The average fiber length (weighted in length) and the average fiber width were 950 µm and 15.6 µm, respectively.

Nitrocellulose membranes of pore size 0.22 µm were supplied by Merck (Darmstadt, Germany). The substrate for the paper dipsticks was uncoated cardboard (160 g m^{-2}) of industrial origin. Oxalic acid, DTZ (≥98%), and methylene blue were purchased from Sigma-Aldrich (Barcelona, Spain). L-ascorbic acid (≥99%) and glacial acetic acid were purchased from Scharlab (Sentmenat, Spain). Ethanol and amylene-stabilized chloroform were received from ThermoFisher Scientific (Loughborough, UK).

$HgCl_2$, $PbCl_2$, $CdCl_2$, $CuCl_2$, $NiCl_2$, $CrCl_3$ and $MgCl_2$ were purchased from Panreac Applichem (Castellar del Valles, Spain); $FeCl_3$, AgCl, $MnCl_2$, $ZnCl_2$ and NaCl were received from Scharlab. The choice of Cl^- as counter-ion is justified by its higher proportion in natural waters (Jin et al. 2019).

Production of nanocellulose

The oxalic acid treatment of cellulose was carried out according to the method outlined by Chen et al. (2016), following the mechanical pretreatment proposed by Bastida et al. (2022). In brief, BEP was initially refined in a PFI mill, undergoing 10000 revolutions. Subsequently, a chemical pre-treatment with 50 wt% oxalic acid was conducted for one hour at 90 ºC (Fig. 1). The carboxyl content was measured by Davidson's methylene blue adsorption method (Davidson 1948).

The fibrillation process was carried out in an NS1001L PANDA 2 K-GEA high-pressure homogenizer (HPH). A suspension of oxidized fibers was passed 3 times at 30 MPa, 3 times at 60 MPa and 3 times at 90 MPa.

For 20 min, an aqueous suspension of ox-CNFs (0.1 wt%) was centrifuged at 2800 g for the gravimetric estimation of the nanofibrillation yield. The dry weight of the supernatant was calculated by subtracting the weight of the centrifugation sediment (W_f) from the initial weight (W_i), based on the following equation:

$$Yield\ (\%) = \left[\frac{W_i - W_f}{W_i}\right] * 100 \quad (2)$$

The transmittance at 600 nm and the cationic demand were measured as described elsewhere (Serra-Parareda et al. 2021a). Hydrodynamic size was determined using a Zetasizer Nano (ZEN 3600, Malvern, UK). The content of carboxylate groups of the oxidized pulp was estimated by the methylene blue adsorption method and the cationic demand was determined by potentiometric back titration.

The limiting viscosity number (η) was measured by the capillary viscometer method, using copper(II) ethylenediamine as solvent as indicated by the ISO standard 5351 (International Standardization Organization 2010). The average molecular weight (weighted in weight, M_w) was estimated therefrom, using the Mark-Houwink parameters provided by Eckelt et al. (2011).

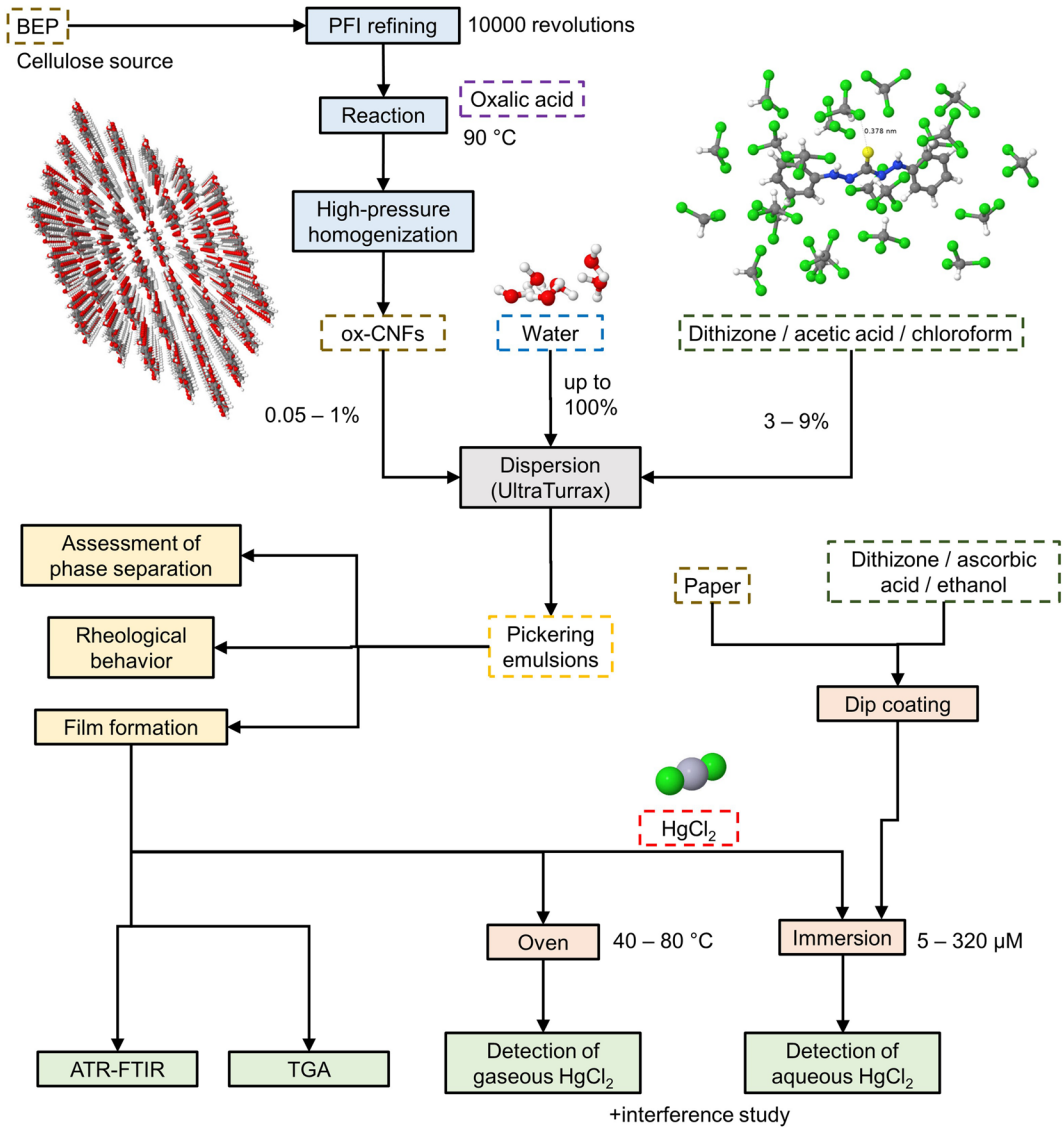

Fig. 1 Scheme of the experimental procedure. Dashed lines present materials, while continuous line frame techniques or operations

The remaining hemicellulose was assessed by ion chromatography, identifying the different monosaccharide constituents after acid hydrolysis (Lamb et al. 1993). This hydrolysis was performed by the two-step procedure described in NREL/TP-510–42618 (Sluiter et al. 2012). Briefly, a sample of ox-CNFs was depolymerized with aqueous H_2SO_4 (72 wt%), at 30 °C, for 1 h. Then the mixture was diluted to 4 wt% H_2SO_4 and autoclaved for 1 h at 121 °C. Finally, the hydrolysate was analyzed by means of a Dionex ICS-5000 DP chromatograph with an anion exchange column and an amperometric detector.

Impregnation of paper with dithizone

0.03 g of DTZ and 0.2 g of ascorbic acid were dissolved in 100 mL of ethanol (96 vol%). To a certain extent, ascorbic acid has been found to be a useful preservative agent for DTZ (Takahashi et al. 2009). In any case, this solution was used for paper impregnation during the same day. Unsized cardboard was cut into strips of (200×20) mm and immersed in the aforementioned DTZ solutions for 20 s. They were then dried by means of a domestic thermoventilator at 50–55 °C.

Preparation of emulsions

DTZ (1.5 g) was dissolved in a mixture of 98 mL of chloroform with 2 mL of acetic acid, a medium that has been proven successful for DTZ storage (Thiagarajan and Subbaiyan 1992). Emulsions were prepared by dispersing 1.2, 2.4 and 3.6 g of DTZ/chloroform in enough water to make up to 40 g, using ox-CNFs (0.05 – 1.0 wt%) as stabilizing agent. Mixtures were stirred at 8000 rpm for 1 min using an UltraTurrax T25 device from IKA (Staufen, Germany). It can be noted that lower mixing intensity did not suffice to attain macroscopic homogeneity, but higher speeds or longer times also increased the undesired generation of stable foam.

After 24 h, emulsions were photographed in a LED-illuminated light box (color temperature 6000 K, surface luminance 310 cd m^{-2}) to identify the critical concentration of ox-CNFs that attained macroscopic homogeneity. Moreover, they were visualized with a DMR-XA optical microscope from Leica (Wetzlar, Germany), placing a coverslip over a drop of non-diluted emulsion in each case. Samples were observed with halogen illumination over bright field and with polarized light and differential interference contrast.

Emulsions were kept at room temperature (25 °C) and in transparent polypropylene tubes. The room did not have any source of ultraviolet radiation, but it had cool white LED illumination (2850 lm). Unlike in a previous work with DTZ/chloroform (Aguado et al. 2023a), an in-depth analysis of chemical stability upon storage is out of the scope. Nonetheless, the absorbance at 608 nm of chloroform extracts was also measured by means of a Shimadzu spectrophotometer UVmini-1240 after different storage times. The chloroform-to-emulsion volume ratio was 25.

For a shear rate range comprising from 0.05 s^{-1} to 50 s^{-1}, the apparent viscosity and the shear stress of nanocellulose-stabilized emulsions were measured using a modular compact rheometer, model MCR 302e, from Anton Paar (Graz, Austria). The module for concentric cylinders was installed and the temperature was kept at 20 °C.

Production of nanocellulose-based films by casting

The emulsions with the highest concentration of ox-CNFs (1.0 wt%) were then cast on nitrocellulose membranes and dried at room temperature for 48 h. The resulting films were conditioned at 25 °C and 50% RH for at least 24 h before testing.

Fourier transform infrared spectroscopy (FTIR) spectra were collected by means of a Bruker Alpha FT-IR spectrometer equipped with an attenuated total reflectance (ATR) accessory, with a resolution of 4 cm^{-1} (Figure S2, SM-1). The thermal degradation behavior was evaluated by means of a thermogravimetric analyzer from Mettler Toledo (Cornellà de Llobregat, Spain), model TGA/DSC1, from 30 to 600 °C at a heating rate of 10 ºC min^{-1}, and both under inert (nitrogen) and oxidizing (air) atmosphere.

Response to heavy metal chlorides in solution

DTZ-impregnated paper strips were dipped into Millie-Q® water to observe the blank signal and calculate its standard deviation. This immersion lasted 20 s and samples were air-dried before colorimetric assays. The same operation was repeated with nanocellulose-based films, similarly, cut as strips without detachment from the nitrocellulose membrane.

Aqueous stock solutions of 100 mg L^{-1} in concentration were prepared from each of the metal chlorides. Paper strips and nanocellulose-based films were dipped into water and in metal chloride solutions as described above for the blank. Metal salts whose mean response was not statistically different from that of the blank were deemed non-interfering at trace concentration. $HgCl_2$, which displayed the strongest signal, was used for quantification, and thus solutions from 2.5 µM (0.68 mg L^{-1}) to 250 µM (68.0 mg L^{-1}) were also prepared.

Detection of sublimated $HgCl_2$

Membranes, once detached from nitrocellulose, were placed in sublimation chambers containing 100 mg of solid mercury(II) chloride. In turn, chambers were put inside an oven. They were submitted to colorimetric assays after 24 h and 48 h. The three dosages of DTZ/chloroform (3, 6, and 9 wt%) were tested, and so were three different temperatures: 40 °C, 60 °C, and 80 °C.

For interference studies, other chlorides of soft Lewis acids besides mercury(II), namely those of lead(II), cadmium(II), and silver(I) were also tested.

Colorimetric assays

CIE 1976 L*a*b color coordinates were read by using an X-Rite RM200 device (Grand Rapids, MI, USA). Calibration was performed over a white surface (L* = 100, a* = b* = 0). These measurements were carried out both for strips immersed in aqueous samples and for films exposed to sublimated heavy metals. In the case of strips, the camera of the device was placed on the tip of the probe after drying. Moreover, the same colorimeter was used to assess the effects of storage time at 23 °C, at 50% relative humidity, and under cool white LED light on the optical properties of the films.

Computational tools

As a proxy for an oxalic acid-treated nanofiber, we edited a cellulose crystallite PDB from the user-friendly tool Cellulose-Builder (Gomes and Skaf 2012). Its topology was generated with the GLYCAM06 force field (Kirschner et al. 2008). A chloroform PDB file and the corresponding ITP code were downloaded from the University of Queensland's Automated Topology Builder (University of Queensland 2023). The structure and topology files for DTZ were retrieved from a previous work (Aguado et al. 2023a). Solvation and equilibration (298 K, 1 bar) were carried out in GROMACS, choosing TIP3P as water model, and the different phases were assembled by Packmol (Martínez et al. 2009).

Results and discussion

Properties of oxalic acid-treated nanofibers

The hydrolysate from ox-CNFs contained 88.02 wt% glucose and 11.84 wt% xylose over the total sugar content, with arabinose, mannose, and glucuronic acids lying below the detection limit. Although the remaining hemicellulose content (specifically, xylan) after the oxalic acid treatment was higher than expected, the discussion will mostly revolve around the main component (cellulose).

Key properties of ox-CNFs, in comparison to TEMPO-oxidized CNFs, are displayed in Table 1. The nanofibrillation yield and the transmittance of the former were lower than those of the latter, likely due to the fraction of microfibers that resisted HPH. The disparity between the cationic demand and the $–COO^-$ content in ox-CNFs indicates a relatively high specific surface area, as this difference has been shown to be indicative of the number of accessible hydroxyl groups by ion–dipole interactions (Serra-Parareda et al. 2021a). Such difference is even greater in the case of TEMPO-oxidized CNFs, but this was expected from the electrostatic repulsion between carboxylate groups. Likewise, it can be stated that acid hydrolysis prevailed over Fischer esterification during the oxalic acid treatment of cellulose. While substitution was exerted to a low extent, given that 111 μmol $–COO^-$ g^{-1} corresponds to a degree of substitution of roughly 0.02, depolymerization took place to the point that the M_w of oxalic acid-treated nanocellulose was $3.65 \cdot 10^4$ g/mol. It can be noted that TEMPO-oxidized nanofibers, having undergone identical pressurization (HPH), displayed a higher average M_w

Table 1 Properties of oxalic acid-treated nanocellulose, compared to the oxidized cellulose nanofibers that were used to emulsify chloroform in a previous work (Aguado et al. 2023a)

Treatment before HPH	TEMPO-mediated oxidation with 5 mmol NaClO g^{-1}	Oxalic acid (50 wt%) treatment (this work)
Nanofibrillation yield (%)[a]	> 95	77.5 ± 0.2
Transmittance at 600 nm (%)[a]	68.0	64.9
Average d_H (nm)[b]	543 ± 20	288 ± 4
Diameter (nm)	25 – 40	6 – 20
Carboxyl content (mmol g^{-1})[a]	0.111 ± 0.008	0.73 ± 0.01
Cationic demand (meq g^{-1})[a]	0.58 ± 0.02	1.29 ± 0.05
η (mL g^{-1})[b]	237	142
Average M_w (g mol^{-1})[b]	$6.31 \cdot 10^4$	$3.65 \cdot 10^4$

[a]Values are the average of two replicates

[b]Values are the average of three replicates

(Table 1). It should be noted that the Mark-Houwink parameters corresponded to cellulose (Eckelt et al. 2011), neglecting the contribution of xylan in this estimation.

The higher hydrodynamic diameter (d_H) of TEMPO-oxidized CNFs can be partially explained by their longer chains (higher M_w), although their larger hydration shells (more carboxylate groups) can exert non-negligible effects on DLS measurements. Evidently, given that the sphericity of nanofibers (of any kind) is far less than unity, the actual diameter is much lower. From transmission electron microscopy images (Bastida et al. 2022), the width of at least 95% of ox-CNFs fell within the 6 – 20 nm range, while their length ranged from 300 nm to 1.2 µm. In comparison, TEMPO-oxidized cellulose nanofibers were thicker and longer, with similar aspect ratios but with diameters in the 25 – 40 nm range (Sanchez-Salvador et al. 2021a, b).

All considered, it could be said that the key properties of ox-CNF suspensions are found in between those of TEMPO-oxidized CNFs and those of nominally neutral CNFs obtained by mechanical defibrillation, e.g., by using super mass colliders (Borsoi et al. 2016).

Assessment of nanocellulose-stabilized emulsions

The DTZ/chloroform phase, constituting 3, 6 or 9 wt % of the mixture, was quickly emulsified in water with ox-CNFs. The height of the emulsified phase showed an increase with stabilizer concentration, which is consistent with typical findings in numerous studies on Pickering stabilization (Courtenay et al. 2021). For CNF consistencies equal to or higher than 0.35 wt%, nearly the whole mixture was stabilized, not observing separation between serum and oil phase, as displayed in Fig. 2.

Even after at least three weeks at room temperature, the mixtures contained no oil phase (or non-emulsified chloroform). However, in no case did the whole volume (100%) attain macroscopical homogeneity, due to a stable foam layer in which chloroform-air interfaces partially replaced chloroform-water interfaces. This layer arose from the fact that the surface tension at the chloroform-air interface (27 mN m^{-1} at 25 ºC) is notably lower than that of water (72 mN m^{-1} at 25 ºC) (Karagianni and Avranas 2009). Although it meant more exposure of DTZ to air, the chloroform-based solvation shell protected DTZ from aerial oxidation or other kinds of degradation during at least three weeks. As found in the previous work with TEMPO-oxidized nanofibers (Aguado et al. 2023a), the maximum absorbance of visible light was located at *ca.* 608 nm (corresponding to chloroform as solvent). After 21 days, the absorbance of chloroform extracts at that wavelength decreased by 13% – 17% (Table S1), but DTZ was still usable as chromogenic reagent.

Figure 3 displays some optical microscopy images, both with halogen illumination and with polarized light. The latter configuration helps visualize

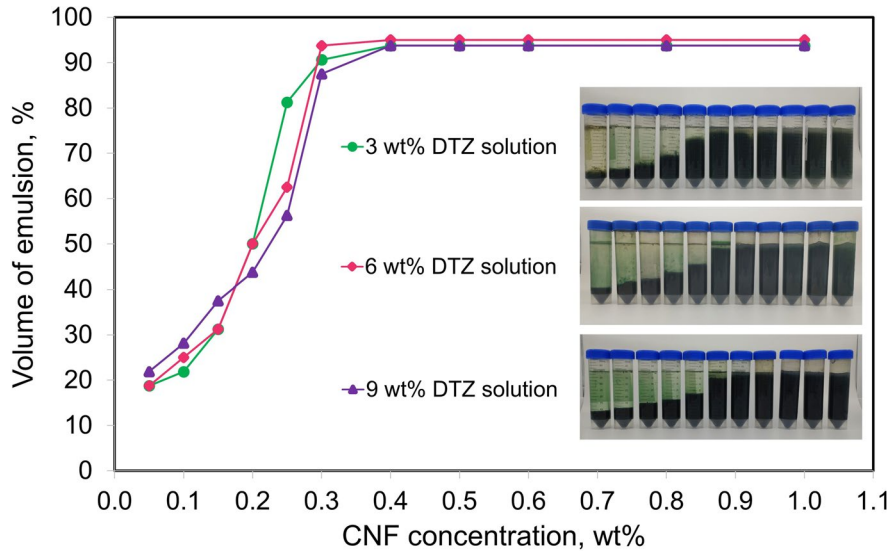

Fig. 2 Proportional volume occupied by the emulsified phase, depending on the nanocellulose concentration for 3, 6 and 9 wt% of DTZ solution. Inset pictures display the nanocellulose-stabilized emulsions and pseudo-emulsions in order of increasing stabilizer concentration

oxalic acid-treated cellulose microfibers, owing to birefringence (Fig. 3a). Nanofibers could not be distinguished at these levels of magnification. The fact that the microfibrillated fraction was not evenly distributed may indicate certain preference for water-chloroform interfaces, due to the amphiphilic character that remains in oxalic acid-treated cellulose. Emulsions were highly polydisperse (Fig. 3b), with the disperse phase comprising a broad size distribution: from small spherical droplets (diameter < 5 μm) to large drops (diameter > 20 μm). In fact, the presence of droplets in the nanoscale, undistinguishable at these levels of magnification, cannot be ruled out. However, there was a physical limit to coalescence, in light of the frequent occurrence of doublets (Figs. 3c and d) that did not become big singlets. Additional micrographs can be found in Figure S1.

Rheological behavior

Starting at 0.35 wt%, ox-CNFs became well-dispersed over the whole volume of the system, generating a significant yield stress. Figure 4 shows the rheological behavior of the critically stabilized emulsions at 20 °C. As generally found for suspensions of nanofibrillated cellulose (Aguado et al. 2023b), there were at least two differentiated regions as a function of the shear rate ($\dot{\gamma}$): viscoelastic behavior for $\dot{\gamma} < 0.05$ s^{-1}

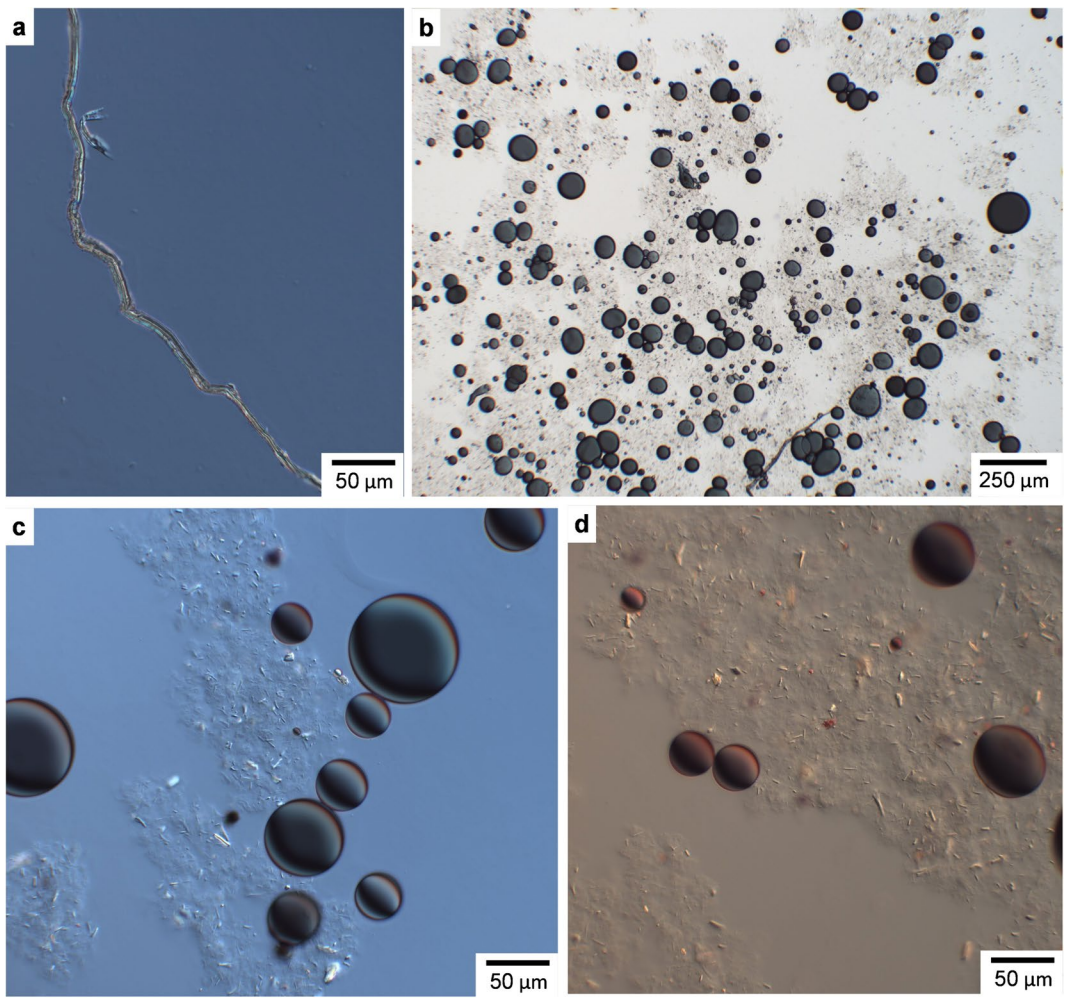

Fig. 3 Optical micrographs of an oxalic acid-treated fiber (**a**); DTZ/chloroform (9 wt%) emulsified in water with ox-CNFs (0.35 wt%), seen under halogen light (**b**); the same emulsion under polarized light (**c**), and DTZ/chloroform (6 wt%) emulsified in water with ox-CNFs (0.35 wt%), seen under polarized light (**d**)

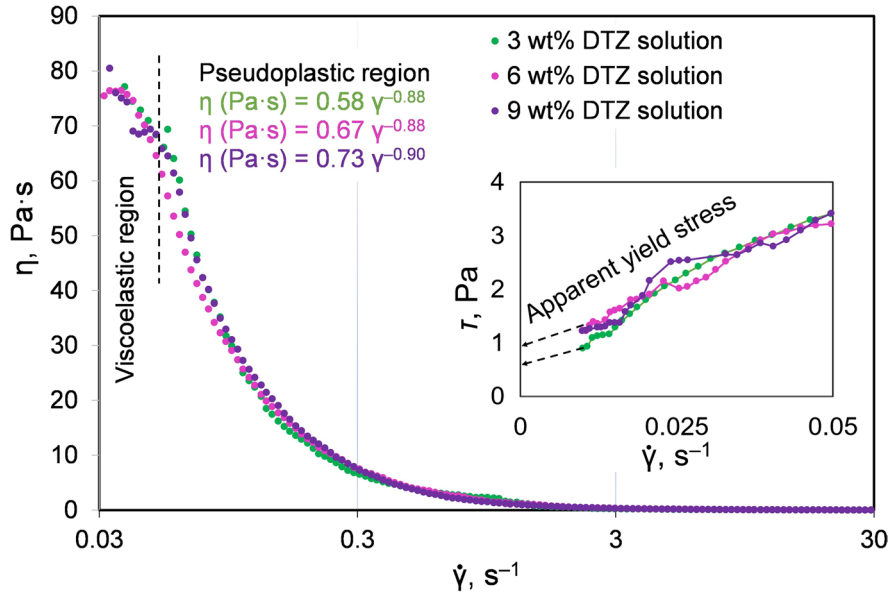

Fig. 4 Rheological assessment of DTZ/chloroform-in-water emulsions stabilized with the minimum dose of ox-CNFs required (0.35 wt%): evolution of the apparent viscosity (main chart) and of the shear stress (inset graph) with the shear rate

and pseudoplastic behavior for $\dot{\gamma} > 0.05\ s^{-1}$. From the viscoelastic region, extrapolating the shear stress (τ) for $\dot{\gamma} = 0$, the yield stress could be estimated as 1.0 Pa for 6 wt% or 9 wt% DTZ/chloroform. It was 0.7 Pa for the lowest proportion of DTZ/chloroform (inset graph in Fig. 4), but it still sufficed to prevent phase separation. The apparent viscosity (η) of emulsions in the pseudoplastic region could be fitted to the Ostwald-De Waele model (Serra-Parareda et al. 2021b):

$$\eta = K\ \dot{\gamma}^{(1-n)} \tag{3}$$

where K is the consistency index and n is the flow behavior index. While there was little influence of the proportion of dispersed phase on viscosity at a given shear rate, increasing this proportion had a consistent positive effect on the consistency index: K = 0.58 Pa·s^n for 3 wt% DTZ/chloroform, K = 0.67 Pa·s^n for 6 wt% DTZ/chloroform, and K = 0.73 Pa·s^n for 9 wt% DTZ/chloroform ($0.3\ s^{-1} < \dot{\gamma} < 30\ s^{-1}$). The pseudoplastic behavior at these levels of shear rate was evidenced by the low values of n: 0.10 – 0.12.

Martins et al. (2022), who used cellulose nanofibers to emulsify soybean oil in water, found similar values for the apparent yield stress (roughly 1 Pa) and for K (0.42 Pa·s^n). Both are relevant for stabilization, since even if the excess gravitational force overcomes the former, the motion would be opposed by a drag force that is roughly proportional to K (Ceylan et al. 1999).

Insights on the stabilization mechanism

The presence of non-coalescing primary doublets in Fig. 3 indicates, in accordance with the DLVO theory, that there was a potential energy barrier at the interface (Derjaguin and Landau 1993; Hatchell et al. 2022). This barrier was due to the electrostatic repulsion between adsorbed ox-CNFs at the interface. However, only large drops formed stable doublets, suggesting that adsorption was stable only when the Sauter radius (R) was high enough (Capron et al. 2017):

$$E_d = \pi\ R^2\ ITF\ (1 - \cos\theta)^2 \tag{4}$$

In Eq. 4, E_d is the energy of desorption; θ is the angle between the tangent line to the oil/water interface and the tangent line to the solid/water interface; ITF is the oil/water interfacial tension, which is 18.2 mN m^{-1} for the chloroform/water interface at pH 5 (Bumbac et al. 2018).

From Fig. 2, the fraction of emulsified chloroform was not dependent on the stabilizer-to-oil ratio, a key parameter when adsorption is the primary mechanism preventing oil droplets from coalescing (Kalashnikova et al. 2013). Instead, it depended only on the concentration of stabilizer, regardless of the concentration of chloroform.

Finally, from Fig. 4, the fact that the apparent viscosity of the emulsions did not decrease with

increasing proportions of the oil phase indicates that droplets did not capture nanofibers onto their surfaces to a great extent. Importantly, if the medium had the rheological behavior of water, all droplets with diameter greater than 1 μm would sediment, given the density of chloroform ($\rho = 1.48$ g cm^{-3}). In other words, gravitational forces would outweigh Brownian motion and Stokes' drag (Mishchuk 2004). Nonetheless, no significant motion (neither random nor gravitational) was detected when observing the droplets of Fig. 3, due to the yield stress. In other words, the thickening behavior of ox-CNFs was deemed the primary stabilization mechanism, with interfacial adsorption being limited to large droplets (Capron et al. 2017).

This does not mean that adsorption at the chloroform/water interface was irrelevant; in fact, it imposed a restriction on the growth of DTZ/chloroform drops. Adsorption in aqueous media can be postulated to be the result of both enthalpic and entropic contributions. On one hand, the large interfacial area that big droplets offer enabled the additive effect of many relatively weak interactions. On the other hand, entropic strive was an important driving force, as indicated by both experiments and molecular dynamics simulations with cellulose-stabilized emulsions (Lee et al. 2021; Kontturi et al. 2024). Briefly put, there is an entropy gain in the system, and thus a decrease in free energy, by the displacement of water from interfaces.

The critical radius for a particle to stay at zero relative velocity (with respect to the continuous phase) can be roughly estimated from the excess gravitational force on the sphere and the yield stress (τ_0). Darby (2000) proposed the stability parameter Y for solid suspensions:

$$Y = \tau_0/[2\,R(\rho - \rho_{water})g] \quad (5)$$

Empirically, if $Y > 0.2$, a particle is expected to stay suspended. From Eq. 5, if $g = 9.81$ m s^{-2}, then the critical condition is given by $R = 364$ μm. All particles smaller than that will not sediment. It can be noted that this radius is much greater than that of the largest drops observed in Fig. 3.

Without any purpose of scale equivalence, a tentative model for the emulsions and films at a molecular level is illustrated in Fig. 5, with each phase equilibrated at 298 K and 1 bar (SM-2). Briefly described, chloroform droplets have their movement restrained by hydrated ox-CNFs in their vicinity. While nanofibers are generally on the aqueous side, DTZ is generally solvated by chloroform. When drying at room temperature to form films, both chloroform and water evaporate to a certain extent, but at least the first hydration layer of ox-CNFs and the solvation shell of DTZ remain.

On the chemical and thermal stability of nanopapers

DTZ/ox-CNF films had certain advantages over DTZ/ethanol-coated paper strips, namely their higher chemical stability towards moisture, air, and heat. This chemical stability was essential for their chromogenic potential. Nanocellulose-supported nanopapers did hardly suffer from color change over at least three weeks (Table S2). In contrast, papers impregnated with DTZ/ethanol suffered from a significant decrease in L* (darkening) and b* (yellowing) color coordinates when exposed to air at 23 °C and 50% relative humidity for 24 h. Likewise, their response to $HgCl_2$ at a given concentration was less noticeable.

To a limited extent, the addition of L-ascorbic acid slowed down the fast degradation of DTZ (Aguado et al. 2023a). It is postulated to have a two-fold mechanism: acidity shifts tautomerism towards the protonated form of dithizone, while the sacrificial oxidation of ascorbate somewhat prevents the aerial oxidation of DTZ. In this sense, the preservative action of L-ascorbic acid has been found to be significantly higher than that of HCl (Takahashi et al. 2009). However, it did not suffice to provide long-lasting stability to DTZ-coated paper strips, probably because it did not protect DTZ from other kinds of degradation in protic solvents (von Eschwege et al. 2011).

Since L-ascorbic acid is not soluble in chloroform, it was not considered for emulsions. Instead, the stability of chloroform-solvated DTZ is granted by acetic acid, as shown by Thiagarajan and Subbaiyan (1992). They suggested that acetic acid prevented the transitory generation of phosgene, which accepted a proton from dithizone. However, in our case, with so much water in the medium, the OH^- ion seems a more plausible proton acceptor. Regardless of the subtleties of the mechanism, the solubility of acetic acid in both phases was of great importance to prevent the deprotonation of DTZ. This way, the loss of absorbance at 608 nm during three weeks was reduced from 47 to 17% with the incorporation of acetic acid (Table S1).

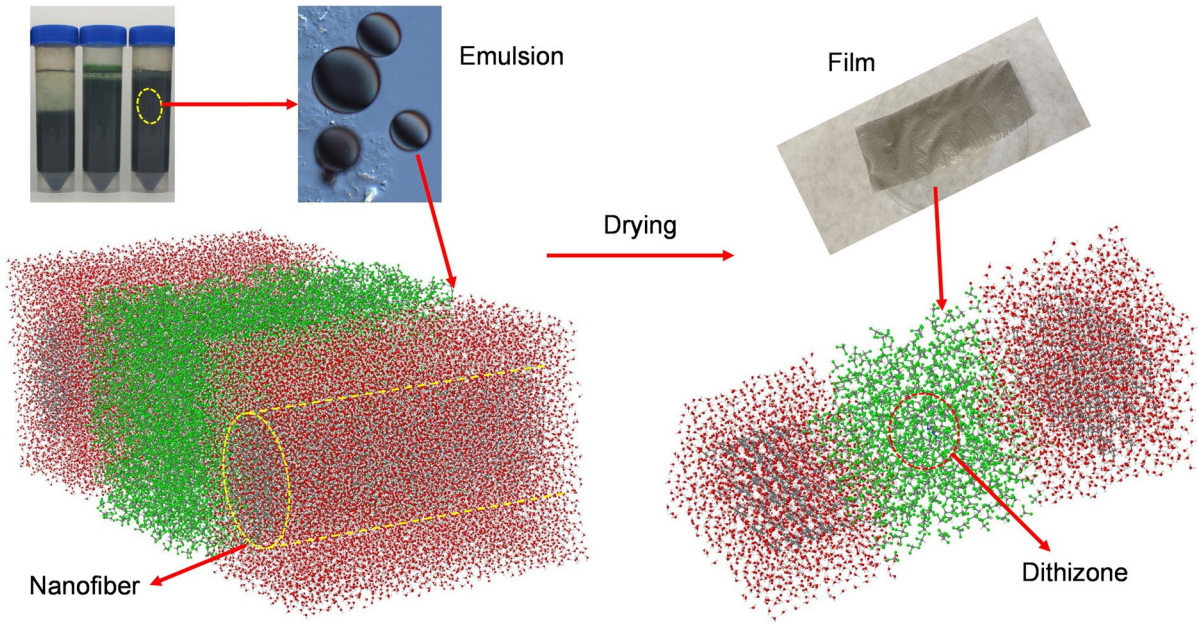

Fig. 5 Simplified molecular modelling of emulsions (left) and films or dipsticks (right). The dimensions of the boxes are (30.0×8.6×10.8) nm and (14.1×6.2×6.2) nm (right)

The results of the thermogravimetric analysis for a given DTZ/ox-CNF film are shown in Fig. 6. The thermograph reveals a weight loss of 9% up to approximately 150 °C, assigned to the desorption of the water and chloroform from the film. Furthermore, two maximum degradation rates are identified in the differential thermal analysis (DTA), one at 345 °C (regardless of the atmosphere), and the other at 452.5 °C for air and at 502 °C for N_2. Thermal decompositions in these regions can be associated with cellulose and dithizone, respectively. During the decomposition of the film, the first significant event is characterized by a weight loss of approximately 58%. Subsequently, in the second event, around 33% of the remaining weight is lost. As previously mentioned, $HgCl_2$-catalyzed industries typically operate within the temperature range of 80 to 180

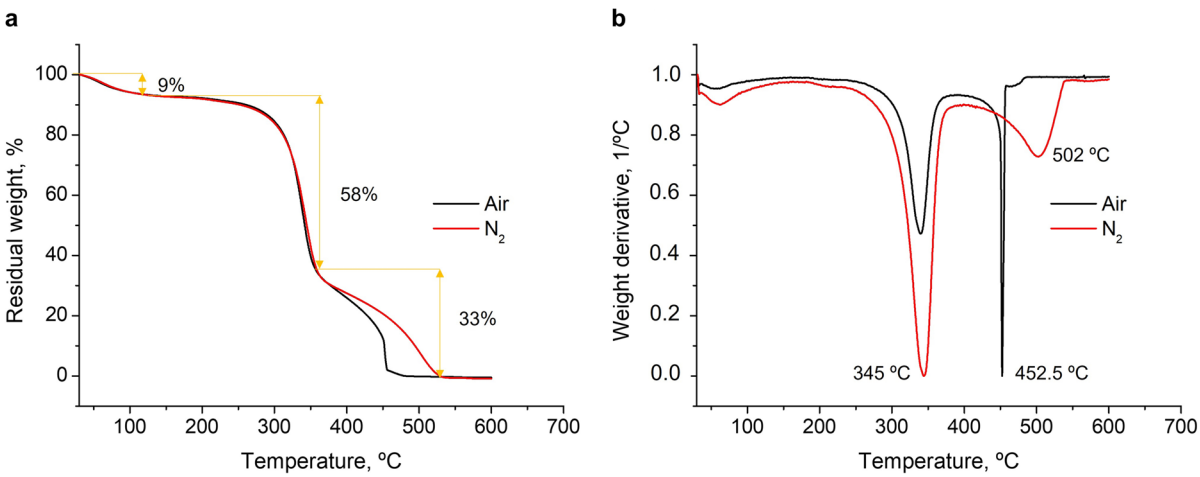

Fig. 6 TGA (**a**) and DTA (**b**) curves of a DTZ/ox-CNF film. The preparation involved ox-CNFs (1.0 wt%), DTZ/chloroform (6 wt%), and water. The percentage of material degraded and the temperature at maximum degradation rate are shown

ºC. From the TGA results, it can be stated that DTZ/ox-CNF films begin to thermally decompose above the operating temperature for the applications studied herein. However, the loss of solvents (including chloroform) starts taking place even below 80 °C, harming the chemical stability of DTZ. Hence, if applied in a vinyl chloride production site, the films should be located outside the hydrochlorination unit, detecting potential leaks of corrosive sublimate but not exposed to its operating temperature.

Colorimetric detection of aqueous mercury(II) chloride

Even though DTZ/ethanol-coated paper strips had to be used during the same day to preserve the chromogenic activity of DTZ, it can be said that they outperformed nitrocellulose-supported DTZ/ox-CNF films in analytical terms.

The color change of DTZ/ethanol-impregnated dipsticks was triggered as soon as each strip was immersed into $HgCl_2$ solutions, as shown in SM-3 (video). In general, this change could be described as reddening, although at low concentrations (below 0.1 mM) it was relative to the degree of brightening. This is why Fig. 7 plots the concentration of $HgCl_2$ against $\Delta a^*/\Delta L^*$, *i.e.*, the shift towards red in the red-green axis divided by the increase in brightness. In the case of DTZ/ethanol-coated papers, such increase was actually negative (darkening) for the blank sample and even for concentrations up to 40 µM, due to the solvatochromic effects on DTZ upon immersion in water (Ntoi et al. 2017). This darkening of the blank was avoided by nanocellulose-based systems.

The limit of detection (LOD) of the DTZ/ethanol/paper system in the aqueous phase was 10 µM (Fig. 7a), corresponding to 2.7 mg/L of $HgCl_2$. This value was estimated as the lowest concentration that triggered a response whose 95% confidence interval did not overlap the 95% confidence interval of the blank. Their limit of quantification (LOQ), estimated as the lowest concentration from which on the response could be reliably fitted to a monotonously increasing function, was 20 µM or 5.4 mg/L. Furthermore, there was linearity ($R^2 = 0.9988$) between $\Delta a^*/\Delta L^*$ and $[HgCl_2]$:

$$[HgCl_2]\ (\mu M) = 7.1\ \Delta a*/\Delta L* + 43\ \forall\ 20\ \mu M \le [HgCl_2] \le 100\ \mu M \quad (6)$$

However, for nanocellulose-based films, quantification was hindered by the low reproducibility of the system, mainly due to unpredictable effects on brightness. Still, all samples above 20 µM (or 5.4 mg/L of $HgCl_2$) triggered a change in $\Delta a^*/\Delta L^*$ that was significantly different from that of the blank. All considered, nanocellulose-based films of DTZ/chloroform-in-water emulsions possessed the advantages of durability and low blank signal but could only fulfill the role of qualitative detection of aqueous $HgCl_2$.

Colorimetric detection of gaseous mercury(II) chloride

At 40 °C, 60 °C, and 80 °C, the vapor pressure of $HgCl_2$ is 0.033 Pa, 0.235 Pa, and 1.36 Pa, respectively (Eq. 1). At the same time, adsorption is universally favored at low temperature (Salvestrini et al. 2022), and thus higher vapor pressure does not necessarily imply faster detection. In order to trigger a significant color change, the films had to be placed inside the oven for enough $HgCl_2$ to be cumulatively adsorbed onto them. The whole process could be described as: (i) adsorption onto ox-CNFs; (ii) diffusion through ox-CNFs to reach chloroform-solvated DTZ; (iii) formation of mercury(II) dithizonate, a complex with two deprotonated DTZ ligands per each Hg(II) central atom (Barros et al. 2023).

In general, as evidenced in Fig. 8, reddening was significant in all cases, with $p < 0.05$ for the null hypothesis ($\Delta a^* \le 0$). This change tended to increase with the amount of DTZ in the film, except for the exposure at 40 °C, likely due to the influence of uncomplexed, excess DTZ on color. As expected, it also increased with the exposure time and from 40 °C to 60 °C. No significant difference was consistently found between 60 °C and 80 °C, given the opposite effects of adsorbate concentration and temperature on adsorption equilibria. In

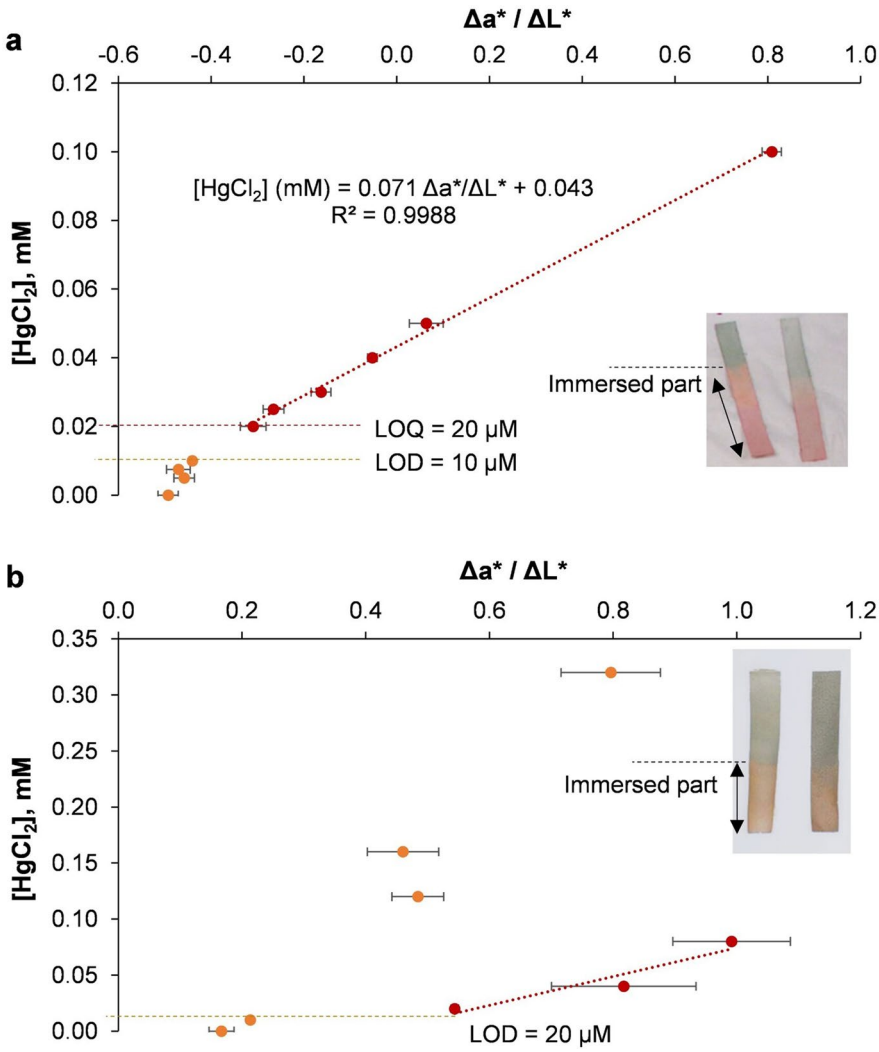

Fig. 7 Colorimetric assessment of $HgCl_2$ in water, using DTZ/ethanol-coated paper strips (**a**) and DTZ/ox-CNF films (**b**). The preparation of the latter involved ox-CNFs (1.0 wt%), DTZ/chloroform (6 wt%), and water at 25 ºC

any case, the effectivity of the system at 60 °C indicates that, assuming ideal gas behavior, concentrations as low as 2.32 ppmv could be detected in an $HgCl_2$-polluted environment. Exposing the films to temperatures above 80 °C is not recommended, since the loss of solvation shells by evaporation would hamper their usability.

Interfering metal chlorides

Trace amounts of lead(II) chloride triggered a reddening response in DTZ/ethanol-coated paper dipsticks, not unlike $HgCl_2$. The LOD of the former was estimated as 7.0 mg L^{-1}, in the same order as the latter (10 μM or 2.7 mg L^{-1}). Paper strips were also responsive to solutions of $CdCl_2$ (red), $ZnCl_2$ (pink), $CuCl_2$ (brown), and $NiCl_2$ (brown) below 100 mg L^{-1}. The response of Mn^{2+} to DTZ, documented in ammonia buffer (Ahmadi-Asoori et al. 2021), was not observed here, probably because L-ascorbic acid prevented the deprotonation of DTZ.

As found for DTZ/chloroform-in-water emulsions stabilized by TEMPO-oxidized nanofibers (Aguado et al. 2023a), ox-CNFs enhanced the selectivity of the system to a certain extent. Remarkably, $PbCl_2$ and $CdCl_2$ required concentrations above 100 mg L^{-1} to trigger significant reddening. This was possibly due to lack of diffusion through the ox-CNF network, especially considering that $PbCl_2$ does not tend to dissociate in water and that its mobility is lower than that of free ions. Other than that, the interfering effects of Zn^{2+}, Cu^{2+}, and Ni^{2+} should be mentioned.

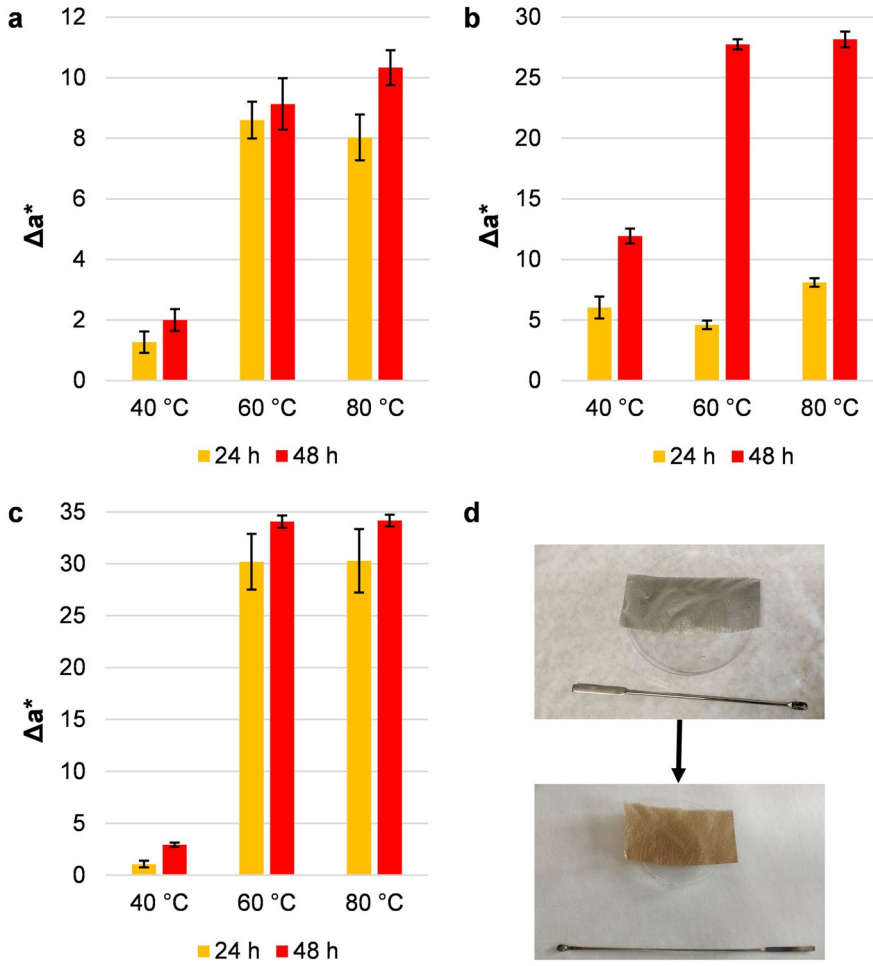

Fig. 8 Reddening of DTZ/ox-CNF films due to the partial sublimation of $HgCl_2$ at 40 °C, 60 °C, and 80 °C. The preparation of these films involved ox-CNFs (1.0 wt%), water, and different proportions of DTZ/chloroform: 3 wt% (**a**), 6 wt% (**b**), and 9 wt% (**c**). Pictures (**d**) exemplify the color change at 60 °C

In other studies with DTZ (without nanocellulose, though), selectivity issues have been traditionally addressed by the addition of another compound, *i.e.*, a masking agent. For instance, if there is ethylenediaminetetraacetic acid (EDTA) in the medium, detection is limited to silver and mercury(II) ions, given that the association constants of other possible targets are higher with EDTA than with DTZ (Irving and Iwantscheff 1980; Cetin et al. 2023).

Regarding the detection of gaseous $HgCl_2$, the system could not be deemed selective by itself, but the vapor pressure at temperatures below 80 °C of other metal chlorides that could trigger a major color change is negligible. That said, we observed certain reddening (up to $\Delta a^* = 7.4$) when exposing the nanopapers to solid $PbCl_2$ for one day at 80 °C, but caution compels us not to rule out the effect of potential impurities.

Conclusions

By combining a classical metallochromic reagent (DTZ) with the usefulness of nanocellulose-stabilized emulsions, this work provided a facile detection system for aqueous and sublimated $HgCl_2$. Solvation of DTZ with acetic acid-containing chloroform granted long-lasting stability upon storage, while oxalic acid-treated nanocellulose worked as the stabilizing agent. Albeit with significant formation of Pickering foam, macroscopic homogeneity was attained as long as the concentration of ox-CNFs was at least 0.35 wt%, regardless of the proportion of DTZ/chloroform in the system. This stabilization was not primarily attributed to interfacial adsorption but to the yield stress (> 0.7 Pa), although electrostatic repulsion played an important role in preventing the coalescence of big droplets. Although this repulsion was lower than

that attained with highly charged TEMPO-oxidized nanofibers, the scarcity of carboxylate groups in ox-CNFs (111 μmol g^{-1}) helped preserve the amphiphilic character of cellulose.

Either as dipsticks for aqueous samples or as membranes for gas detection, colorimetric probes were visually responsive to $HgCl_2$, immediately in the first case and requiring cumulative adsorption in the second case. They attained a LOD of 20 μM for aqueous $HgCl_2$ and required an aerial concentration of nearly 2 ppmv for corrosive sublimate. Nonetheless, this system had limitations that should be addressed by further efforts: the use of a toxic solvent (chloroform) for the sake of DTZ's stability, the interference of other heavy metals (especially in solution), and the lack of immediate response to gaseous $HgCl_2$.

Acknowledgments Authors wish to acknowledge the financial support of the funding agencies listed in the "Funding" section for their support to develop the present work. Furthermore, we are thankful to the Research Technical Services of the University of Girona, particularly to the Unit of Microscopy and the Unit of Thermal Analysis.

Authors' contributions All authors contributed to the conception of the study. The methodology was proposed by Roberto J. Aguado, Quim Tarrés and Nuria Fiol. The preparation of the material, the collection and analysis of data were carried out by Gabriela A. Bastida and Roberto J. Aguado. The first draft of the manuscript was written by Roberto J. Aguado, and all authors commented on earlier versions of the manuscript. Quim Tarrés, María V. Galván, Miguel Á. Zanuttini and Marc Delgado-Aguilar collected all comments and revised the final version of the manuscript, which was read and approved by all authors.

Funding Open Access funding provided thanks to the CRUE-CSIC agreement with Springer Nature. This research was funded by the Spanish Ministry of Science and Innovation, project CON-FUTURO-ES (PID2020-113850RB-C22).

Data availability Raw data of the present work can be made available upon request.

Declarations

Ethics approval and consent to participate Authors declare that the manuscript is not submitted to any other journal at the time of submission for simultaneous consideration, that the submitted work is original and has not been published elsewhere in any form, that this work is not part of a single study, that results are presented under the principles of honesty, without fabrication, falsification or inappropriate data manipulation, and that no data, text or theories by others are presented as our own.

Consent for publication All authors have revised the last version of the submitted manuscript, and we approve its submission.

Competing interests The authors declare no competing interests.

References

Aguado RJ, Mazega A, Fiol N et al (2023) Durable Nanocellulose-Stabilized Emulsions of Dithizone/Chloroform in Water for Hg2+ Detection: A Novel Approach for a Classical Problem. ACS Appl Mater Interfaces. https://doi.org/10.1021/acsami.2c22713

Aguado RJ, Mazega A, Tarrés Q, Delgado-Aguilar M (2023) The role of electrostatic interactions of anionic and cationic cellulose derivatives for industrial applications: A critical review. Ind Crops Prod 201:116898. https://doi.org/10.1016/j.indcrop.2023.116898

Ahmadi-Asoori S, Tazikeh-Lemeski E, Mirabi A et al (2021) Preparation of nanocellulose modified with dithizone for separation, extraction and determination of trace amounts of manganese ions in industrial wastewater samples. Microchem J 160:105737. https://doi.org/10.1016/j.microc.2020.105737

Ashizawa T, Sugizaki S, Asahi H et al (1970) Study of monocolor spectrophotometric determination of lead, zinc and cadmium by dithizone extraction. Bunseki Kagaku 19:1333–1340. https://doi.org/10.2116/bunsekikagaku.19.1333

Barros JDVC, Castro JDS, das Virgens CF (2023) Machine learning approach for ion imprinted (IIP) and non-imprinted (NIP) polymer discrimination based on pyrolysis kinetic data. Polymer (Guildf) 288:126424. https://doi.org/10.1016/j.polymer.2023.126424

Bastida GA, Schnell CN, Mocchiutti P et al (2022) Effect of Oxalic Acid Concentration and Different Mechanical Pre-Treatments on the Production of Cellulose Micro/Nanofibers. Nanomaterials 12:2908

Borsoi C, Zimmernnam MVG, Zattera AJ et al (2016) Thermal degradation behavior of cellulose nanofibers and nanowhiskers. J Therm Anal Calorim 126:1867–1878. https://doi.org/10.1007/s10973-016-5653-x

Bumbac M, Nicolescu CM, Serban BC et al (2018) The interfacial behavior of calixarene and crown ethers at the air/water and chloroform/water interface. J Sci Arts 43:459–470

Capron I, Rojas OJ, Bordes R (2017) Behavior of nanocelluloses at interfaces. Curr Opin Colloid Interface Sci 29:83–95. https://doi.org/10.1016/j.cocis.2017.04.001

Cetin D, Yavuz O, Alcay Y et al (2023) Development of a new near-infrared, spectrophotometric, and colorimetric probe based on phthalocyanine containing mercaptoquinoline unit for discriminative and highly sensitive detection of Ag+, Cu2+, and Hg2+ ions. Spectrochim Acta A Mol Biomol Spectrosc 297:122725. https://doi.org/10.1016/j.saa.2023.122725

Ceylan K, Herdem S, Abbasov T (1999) A theoretical model for estimation of drag force in the flow of non-newtonian fluids around spherical solid particles. Powder Technol 103:286–291. https://doi.org/10.1016/S0032-5910(99)00025-X

Chen L, Zhu JY, Baez C et al (2016) Highly thermal-stable and functional cellulose nanocrystals and nanofibrils produced using fully recyclable organic acids. Green Chem 18:3835–3843. https://doi.org/10.1039/C6GC00687F

Courtenay JC, Jin Y, Schmitt J et al (2021) Salt-Responsive Pickering Emulsions Stabilized by Functionalized Cellulose Nanofibrils. Langmuir 37:6864–6873. https://doi.org/10.1021/acs.langmuir.0c03306

Darby R (2000) Pressure drop for non-Newtonian slurries : A wider path. Chem Eng 107:64–67

Davidson GF (1948) The acidic properties of cotton cellulose and derived oxycelluloses. Part II. The absorption of methylene blue. J Text Inst Trans 39:T65–T86. https://doi.org/10.1080/19447024808659403

de Souza AG, Ferreira RR, Aguilar ESF et al (2021) Cinnamon Essential Oil Nanocellulose-Based Pickering Emulsions: Processing Parameters Effect on Their Formation, Stabilization, and Antimicrobial Activity. Polysaccharides 2:608–625. https://doi.org/10.3390/polysaccharides2030037

Derjaguin B, Landau L (1993) Theory of the stability of strongly charged lyophobic sols and of the adhesion of strongly charged particles in solutions of electrolytes. Prog Surf Sci 43:30–59. https://doi.org/10.1016/0079-6816(93)90013-L

Eckelt J, Knopf A, Röder T et al (2011) Viscosity-molecular weight relationship for cellulose solutions in either NMMO monohydrate or cuen. J Appl Polym Sci 119:670–676. https://doi.org/10.1002/app.32785

Evans WL, Looker CD (1921) THE INFLUENCE OF POTASSIUM HYDROXIDE ON THE FORMATION OF VINYL ALCOHOL FROM ACETALDEHYDE. J Am Chem Soc 43:1925–1928. https://doi.org/10.1021/ja01441a021

Fiol N, Vásquez MG, Pereira M et al (2019) TEMPO-oxidized cellulose nanofibers as potential Cu(II) adsorbent for wastewater treatment. Cellulose 26:903–916. https://doi.org/10.1007/s10570-018-2106-7

Gomes TCF, Skaf MS (2012) Cellulose-Builder: A toolkit for building crystalline structures of cellulose. J Comput Chem 33:1338–1346. https://doi.org/10.1002/jcc.22959

Hatchell D, Song W, Daigle H (2022) Effect of interparticle forces on the stability and droplet diameter of Pickering emulsions stabilized by PEG-coated silica nanoparticles. J Colloid Interface Sci 626:824–835. https://doi.org/10.1016/j.jcis.2022.07.004

International Standardization Organization (2010) ISO 5351:2010(en) Pulps — Determination of limiting viscosity number in cupri-ethylenediamine (CED) solution. ISO TC/6: Paper, Board and Pulps, Geneva

Irving HMNH, Iwantscheff G (1980) The Analytical Applications of Dithizone. C R C Crit Rev Anal Chem 8:321–366. https://doi.org/10.1080/10408348008542714

Isogai T, Saito T, Isogai A (2010) TEMPO Electromediated Oxidation of Some Polysaccharides Including Regenerated Cellulose Fiber. Biomacromol 11:1593–1599. https://doi.org/10.1021/bm1002575

Jin Y, Jin X, Yang D, Mao X (2019) Controlling Factors of Surface Water Ionic Composition Characteristics in the Lake Genggahai Catchment, NE Qinghai-Tibetan Plateau. China Water (basel) 11:1329. https://doi.org/10.3390/w11071329

Kalashnikova I, Bizot H, Bertoncini P et al (2013) Cellulosic nanorods of various aspect ratios for oil in water Pickering emulsions. Soft Matter 9:952–959. https://doi.org/10.1039/C2SM26472B

Karagianni M, Avranas A (2009) The effect of deaeration on the surface tension of water and some other liquids. Colloids Surf A Physicochem Eng Asp 335:168–173. https://doi.org/10.1016/j.colsurfa.2008.11.002

Kirschner KN, Yongye AB, Tschampel SM et al (2008) GLYCAM06: A generalizable biomolecular force field. Carbohydrates. J Comput Chem 29:622–655. https://doi.org/10.1002/jcc.20820

Kontturi KS, Solhi L, Kontturi E, Tammelin T (2024) Adsorption of Polystyrene from Theta Condition on Cellulose and Silica Studied by Quartz Crystal Microbalance. Langmuir 40:568–579. https://doi.org/10.1021/acs.langmuir.3c02777

Lamb JD, Myers GS, Edge N (1993) Ion Chromatographic Analysis of Glucose, Fructose, and Sucrose Concentrations in Raw and Processed Vegetables. J Chromatogr Sci 31:353–357. https://doi.org/10.1093/chromsci/31.9.353

Lee KK, Low DY, Foo ML et al (2021) Molecular Dynamics Simulation of Nanocellulose-Stabilized Pickering Emulsions. Polymers (basel) 13:668. https://doi.org/10.3390/polym13040668

Li X, Zhang H, Man B et al (2018) Synthesis of Vinyl Chloride Monomer over Carbon-Supported Tris-(Triphenylphosphine) Ruthenium Dichloride Catalysts. Catalysts 8:276. https://doi.org/10.3390/catal8070276

Li J, Fan J, Ali S et al (2019) The origin of the extraordinary stability of mercury catalysts on the carbon support: the synergy effects between oxygen groups and defects revealed from a combined experimental and DFT study. Chin J Catal 40:141–146. https://doi.org/10.1016/S1872-2067(19)63271-7

Li J, Wei W, Zhen W et al (2019) How Green Transition of Energy System Impacts China's Mercury Emissions. Earths Future 7:1407–1416. https://doi.org/10.1029/2019EF001269

Li X, Li J, Kuang Y et al (2020) Stabilization of Pickering emulsions with cellulose nanofibers derived from oil palm fruit bunch. Cellulose 27:839–851. https://doi.org/10.1007/s10570-019-02803-4

Martínez L, Andrade R, Birgin EG, Martínez JM (2009) PACKMOL: A package for building initial configurations for molecular dynamics simulations. J Comput Chem 30:2157–2164. https://doi.org/10.1002/jcc.21224

Martins LS, dos Santos RG, Spinacé MAS (2022) Properties of Cellulose Nanofibers Extracted from Eucalyptus and their Emulsifying Role in the Oil-in-Water Pickering Emulsions. Waste Biomass Valorization 13:689–705. https://doi.org/10.1007/s12649-021-01498-8

Mishchuk NO (2004) Coalescence kinetics of Brownian emulsions. In: Petsev DN (ed) Emulsions: Structure, Stability and Interactions. Elsevier, Albuquerque, pp 351–390. https://doi.org/10.1016/S1573-4285(04)80011-5

Naghdi T, Golmohammadi H, Yousefi H et al (2020) Chitin Nanofiber Paper toward Optical (Bio)sensing Applications. ACS Appl Mater Interfaces 12:15538–15552. https://doi.org/10.1021/acsami.9b23487

Ntoi LLA, Buitendach BE, von Eschwege KG (2017) Seven Chromisms Associated with Dithizone. J Phys Chem A 121:9243–9251. https://doi.org/10.1021/acs.jpca.7b09490

Oza KP, Frank SG (1986) Microcrystalline cellulose stabilized emulsions. J Dispers Sci Technol 7:543–561. https://doi.org/10.1080/01932698608943478

Phillips GF, Dixon BE, Lidzey RG (1959) The volatility of organo-mercury compounds. J Sci Food Agric 10:604–610. https://doi.org/10.1002/jsfa.2740101105

Saito T, Isogai A (2004) TEMPO-mediated oxidation of native cellulose. The effect of oxidation conditions on chemical and crystal structures of the water-insoluble fractions. Biomacromol 5:1983–1989. https://doi.org/10.1021/bm0497769

Salvestrini S, Ambrosone L, Kopinke F-D (2022) Some mistakes and misinterpretations in the analysis of thermodynamic adsorption data. J Mol Liq 352:118762. https://doi.org/10.1016/j.molliq.2022.118762

Sanchez-Salvador JL, Campano C, Lopez-Exposito P et al (2021) Enhanced Morphological Characterization of Cellulose Nano/Microfibers through Image Skeleton Analysis. Nanomaterials 11:2077. https://doi.org/10.3390/nano11082077

Sanchez-Salvador JL, Campano C, Negro C et al (2021) Increasing the Possibilities of TEMPO-Mediated Oxidation in the Production of Cellulose Nanofibers by Reducing the Reaction Time and Reusing the Reaction Medium. Adv Sustain Syst 5:2000277. https://doi.org/10.1002/adsu.202000277

Sangvanich T, Morry J, Fox C et al (2014) Novel Oral Detoxification of Mercury, Cadmium, And Lead with Thiol-Modified Nanoporous Silica. ACS Appl Mater Interfaces 6:5483–5493. https://doi.org/10.1021/am5007707

Serra-Parareda F, Aguado R, Tarrés Q et al (2021) Potentiometric back titration as a robust and simple method for specific surface area estimation of lignocellulosic fibers. Cellulose 28:10815–10825. https://doi.org/10.1007/s10570-021-04250-6

Serra-Parareda F, Tarrés Q, Mutjé P et al (2021) Correlation between rheological measurements and morphological features of lignocellulosic micro/nanofibers from different softwood sources. Int J Biol Macromol 187:789–799. https://doi.org/10.1016/j.ijbiomac.2021.07.195

Sharifi AR, Naghdi T, Yousefi H et al (2022) Nanopapers toward Green Photonic and Optical Applications. ACS Sustain Chem Eng 10:16995–17026. https://doi.org/10.1021/acssuschemeng.2c04224

Sluiter A, Hames B, Ruiz R, Scarlata C, Sluiter J, Templeton D, Crocker D (2012) Determination of structural carbohydrates and lignin in biomass. NREL Laboratory Analytical Procedure. www.nrel.gov/bioenergy/biomass-compositional-analysis.html

Takahashi Y, Danwittayakul S, Suzuki TM (2009) Dithizone nanofiber-coated membrane for filtration-enrichment and colorimetric detection of trace Hg(ii) ion. Analyst 134:1380–1385. https://doi.org/10.1039/B816461D

Tang P, Si Y, Song X, Sun G (2024) Hierarchically porous bacterial cellulose nanofibrous membranes for selective adsorption and real-time colorimetric monitoring of volatile carboxylic acids. Cellulose 31:381–393. https://doi.org/10.1007/s10570-023-05632-8

TAPPI (2020) Alpha-, beta- and gamma-cellulose in pulp, Test Method T 203. TAPPI Standards, Technical Information Papers, and Useful Methods. Technical Association of the Pulp & Paper Industry, New York

Thiagarajan N, Subbaiyan M (1992) Stability of dithizone in chloroform-acetic acid solvent system. Anal Chim Acta 269:269–272. https://doi.org/10.1016/0003-2670(92)85412-Y

Tigari G, Manjunatha JG, Raril C (2021) Electrochemical Determination of Indigotine Based on Poly(Gibberellic Acid)-Modified Carbon Nanotube Paste Electrode. In: Mallakpour S, Hussain CM (eds) Environmental Applications of Carbon Nanomaterials-Based Devices, pp 135–146. https://doi.org/10.1002/9783527830978.ch5

Tong Y, Zhang H, Lin H et al (2021) A potential route for photolytic reduction of HgCl2 and HgBr 2 in dry air and analysis about the impacts from Ozone. Atmos Res 249:105310. https://doi.org/10.1016/j.atmosres.2020.105310

Torlopov MA, Vaseneva IN, Mikhaylov VI et al (2021) Pickering emulsions stabilized by partially acetylated cellulose nanocrystals for oral administration: oils effect and in vivo toxicity. Cellulose 28:2365–2385. https://doi.org/10.1007/s10570-021-03690-4

Umar Y (2022) Experimental (FT-IR, FT-Raman, and NMR) and DFT studies of the structures and spectral properties of diphenylcarbazone and diphenylthiocarbazone. J Mol Struct 1264:133230. https://doi.org/10.1016/j.molstruc.2022.133230

University of Queensland (2023) Automated Topology Builder. https://atb.uq.edu.au/. Accessed 11 Dec 2023

von Eschwege KG, Conradie J, Kuhn A (2011) Dithizone and Its Oxidation Products: A DFT, Spectroscopic, and X-ray Structural Study. J Phys Chem A 115:14637–14646. https://doi.org/10.1021/jp208212e

Wang S, Xu Z, Fang Y et al (2018) Development of Cellulosic Paper-Based Test Strips for Mercury(II) Determination in Aqueous Solution. J Anal Methods Chem 2018:3594020. https://doi.org/10.1155/2018/3594020

Ye X, Kang Y, Zhou J (2020) Rhodamine labeled cellulose nanocrystals as selective "naked-eye" colorimetric and fluorescence sensor for Hg2+ in aqueous solutions. Cellulose 27:5197–5210. https://doi.org/10.1007/s10570-020-03126-5

Yu D, Luo Q, Zhang J et al (2022) Pickering emulsions co-stabilised by cellulose nanofibres and nicotinamide mononucleotide. Cellulose 29:8569–8585. https://doi.org/10.1007/s10570-022-04805-1

Zheng Y, Oguzlu H, Baldelli A et al (2022) Sprayable cellulose nanofibrils stabilized phase change material Pickering emulsion for spray coating application. Carbohydr Polym 291:119583. https://doi.org/10.1016/j.carbpol.2022.119583

Marc Delgado-Aguilar and Quim Tarrés are Serra Húnter Fellows.